AEROELASTIC GUST LOAD PREDICTION BASED ON TIME-LINEARIZED RANS SOLUTIONS

C. Kaiser, D. Friedewald, D. Quero, J. Nitzsche
Institute of Aeroelasticity
German Aerospace Center (DLR)
37073 Göttingen, Germany

Abstract

In this paper the multi-disciplinary simulation of unsteady flight maneuvers with a reduced-order model (ROM) based on time-linearized RANS solutions is demonstrated for the analysis of gust encounter of the XRF1 transport aircraft configuration at transonic speed. The numerical prediction of gust loads requires the coupling of the disciplines aerodynamics, structural dynamics and flight mechanics. The aeroelastic coupling is realised in the frequency domain in terms of generalized coordinates and forces employing a fluid-structure feedback loop. The Linear Frequency Domain (LFD) solver of the DLR TAU code is used to construct the linearized aerodynamic reduced-order model. The LFD solver offers a significant reduction in computational effort for small-perturbation problems while completely retaining the fidelity of the Reynolds-averaged Navier-Stokes (RANS) flow solutions. For validation, both the aerodynamic and aeroelastic response due to a 1-cos gust encounter are compared to aerodynamically nonlinear time domain simulations. The coupled aeroelastic model accounts for rigid-body and elastic motion of the aircraft in form of mode shapes for the heave and pitch motion as well as the first elastic wing bending mode.

NOMENCLATURE

α	=	incidence angle
f	=	frequency
$\boldsymbol{K}$	=	modal stiffness matrix
$\boldsymbol{M}$	=	modal mass matrix
Ma_∞	=	freestream Mach number
λ	=	gust wave length
ϕ	=	phase angle
Re_∞	=	freestream Reynolds number
U_∞	=	freestream velocity
v_g	=	grid node velocities
ω	=	angular frequency
w	=	gust velocity
$\boldsymbol{W}$	=	vector of conservative variables
$\boldsymbol{x}$	=	grid node coordinates

Superscripts:

$\dot{}$	=	temporal derivative $\partial/\partial t$
$\bar{}$	=	time-invariant mean state
$\hat{}$	=	perturbation amplitude, Fourier coefficient

Abbreviations:

FRF	=	frequency response function
GAF	=	generalized aerodynamic force
LFD	=	linear frequency domain solver
RHS	=	right-hand-side vector
ROM	=	reduced order model

INTRODUCTION

The computational effort of solving the Reynolds-averaged Navier-Stokes (RANS) equations for the prediction of unsteady airloads remain very high. Hence, considering the huge parameter space for the analysis of the maximum gust loads on an aircraft, faster but less accurate unsteady aerodynamic methods like the doublet lattice method (DLM) are still in wide use. The DLM method [1] is based on the compressible acceleration potential theory and as such it does not account for effects of wing thickness, recompression shocks or boundary layer separation. In contrast, the Linear Frequency Domain (LFD) solver [2] of the DLR TAU code, captures all characteristics of RANS solutions while yet offering a notable reduction in computational effort [3]. Aiming for the aircraft's response to small oscillatory perturbations, the LFD solves for the first harmonic of the flow response. Therefore, the discretized RANS equations are linearized around the steady state and harmonic small-amplitude perturbations of constant frequency are assumed. The frequency-domain approach is well suited for inherently linear problems like the determination of the flutter stability of an aircraft. In contrast, gust simulations are commonly conducted in the time domain in order to account for the large flow perturbations that are caused by a gust. However, by experience, linearized gust simulations in most cases can be assumed to yield conservative results where the linearized time-domain response can be found by the inverse Fourier transform of the frequency-domain gust loads.

The time-linearized approach allows the prediction of a dynamic aircraft response on the basis of a set of aerodynamic linear transfer functions that each link a specific gust or aircraft motion input to a certain

aerodynamic force output. Once established these aerodynamic transfer functions can be easily extended to account for the aircraft's structural dynamic reaction leading to the aeroelastic transfer function. The transfer functions are typically formulated in generalized coordinates and generalized forces.

In this paper, at first, the governing equations of the LFD for forced motion and gust encounters along with the structural dynamic equations are introduced. The investigated gust encounter on the transport aircraft model at transonic cruise is described in the following section. Finally, the linearized aerodynamic and aeroelastic transfer functions and the dynamic aircraft response are validated with nonlinear reference solutions.

1. NUMERICAL METHODS

1.1. Aerodynamic Governing Equations

The governing equations of the DLR TAU flow solver [4] are the Reynolds-Averaged Navier-Stokes (RANS) equations employing an unstructured finite volume discretization. The turbulence closure applied in this paper is the one-equation turbulence model by Spalart and Allmaras [5]. The unsteady RANS computation is performed by the dual-time stepping approach according to Jameson [6] with a second-order backward differencing in time. The governing equations expressed in the discretized integral conservation form can be written with the vector of unknown conservative variables $\boldsymbol{W}$ and the integration matrix $\boldsymbol{V}$ as:

$$(1)\quad \frac{d(\boldsymbol{VW})}{dt} + \boldsymbol{R}\left(\boldsymbol{W}, \boldsymbol{x}, \boldsymbol{v}_g\right) = 0$$

The residual $\boldsymbol{R}$ represents the convective and viscous fluxes including the flux due to additional grid velocities from an Arbitrary Lagrangian-Eulerian extension [7] as well as the sources of the turbulence model. Hence, the residual depends on both the time-dependent grid node coordinates $\boldsymbol{x}(t)$ and the grid node velocities $\boldsymbol{v}_g(t)$. Both variables are required for the computation of moving-grid and gust simulations. Moving-grid simulations comprise of prescribed grid deformations [8] at each time step introducing grid velocities from the changing grid node coordinates. For the simulation of gust encounters, the disturbance velocity approach [9][10] allows to directly introduce the gust induced velocities as negative grid node velocities.

1.2. Linear Frequency Domain Solver

The linear frequency domain solver (LFD) is an extension of the DLR TAU code which solves for the first-harmonic small-disturbance solution of the RANS equations [2]. Therefore, the governing equations are linearized around the steady flow state by the truncated Taylor series expansion with only small-harmonic perturbations of the steady flow field: $\boldsymbol{W}(t) \approx \overline{\boldsymbol{W}} + \widehat{\boldsymbol{W}} e^{i\omega t}$. These perturbations are induced by small-harmonic grid node movements of amplitudes $\hat{\boldsymbol{x}}$ or $\widehat{\boldsymbol{v_g}}$ due to grid motion or gust encounters After the linearization and under the assumption of a zero steady-state residual $\boldsymbol{R}\left(\overline{\boldsymbol{W}}, \overline{\boldsymbol{x}}, \overline{\boldsymbol{v_g}}\right) = 0$ equation (1) is expressed in form of a linear system of equations for the unknown complex-valued first-harmonic amplitudes of the conservative variables $\widehat{\boldsymbol{W}}$:

$$(2)\quad \boldsymbol{A}\widehat{\boldsymbol{W}} = \boldsymbol{b}$$

The system matrix $\boldsymbol{A}$ consists of the Jacobian of the residual evaluated at the steady-state, the steady-state integration matrix $\overline{\boldsymbol{V}}$ and the harmonic excitation frequency ω:

$$(3)\quad \boldsymbol{A} = i\omega\overline{\boldsymbol{V}} + \frac{\partial \boldsymbol{R}}{\partial \boldsymbol{W}}\Big|_{\overline{\boldsymbol{W}}, \overline{\boldsymbol{x}}, \overline{\boldsymbol{v}_g}}$$

The Jacobian matrix has been derived analytically for the DLR TAU code [11] including the applied turbulence model of Spalart and Allmaras. The right-hand side (RHS) vector $\boldsymbol{b}$ comprises the remaining terms from the truncated Taylor series expansion involving the excitation perturbations of the grid node locations $\hat{\boldsymbol{x}}$ and grid node velocities $\widehat{\boldsymbol{v}_g}$:

$$(4)\quad \boldsymbol{b} = -\left(\frac{\partial \boldsymbol{R}}{\partial \boldsymbol{x}}\Big|_{\overline{\boldsymbol{W}}, \overline{\boldsymbol{x}}, \overline{\boldsymbol{v}_g}} + i\omega\overline{\boldsymbol{W}}\frac{\partial \boldsymbol{V}}{\partial \boldsymbol{x}}\Big|_{\overline{\boldsymbol{x}}}\right)\hat{\boldsymbol{x}} - \frac{\partial \boldsymbol{R}}{\partial \boldsymbol{v}_g}\Big|_{\overline{\boldsymbol{W}}, \overline{\boldsymbol{x}}, \overline{\boldsymbol{v}_g}}\widehat{\boldsymbol{v}_g}$$

For moving-grid simulations, the RHS vector is defined by the vector of amplitudes $\hat{\boldsymbol{x}}$ from the grid deformation yielding the grid node velocities $\widehat{\boldsymbol{v}_g} = i\omega\hat{\boldsymbol{x}}$. In case of harmonic gust simulations, there is zero grid movement $\hat{\boldsymbol{x}} = 0$ and the grid node velocities result from the harmonic gust velocity profile with the real-valued amplitude $\hat{\boldsymbol{w}}$:

$$(5)\quad \widehat{\boldsymbol{v}_g} = -\hat{\boldsymbol{w}} e^{i\phi(\boldsymbol{x})}$$

Equation (5) includes a phase shift which follows from the travelling movement of the harmonic gust field in the time domain [12]. Hence, the phase shift depends on the spatial distance from a reference point $\boldsymbol{x}_0$ which can be considered as a starting point of the gust in the time-domain:

$$(6)\quad \phi(\boldsymbol{x}) = 2\pi\frac{\boldsymbol{x}_0 - \boldsymbol{x}}{\lambda}$$

The derivatives of the residual in equation (4) are evaluated by central finite differences. Finally, the linear equation system (2) is solved iteratively with a Krylov generalized minimum-residual scheme (GMRES) [13] and incomplete lower-upper preconditioning [14].

1.3. Structural Dynamic Governing Equations

For the aeroelastic computation, the second-order, linear structural equations of motion coupled with the aerodynamic forces can be expressed as:

$$(7)\quad \boldsymbol{M}\ddot{\boldsymbol{q}}(t) + \boldsymbol{K}\boldsymbol{q}(t) = \boldsymbol{GAF}(t) = \boldsymbol{\Phi}^{\mathrm{T}}\boldsymbol{f}_a(t)$$

The modal mass matrix $\boldsymbol{M}$ and the modal stiffness matrix $\boldsymbol{K}$ account for both the rigid body motion and the elastic displacements. The aerodynamic forces $\boldsymbol{f}_a$ on the aerodynamic surface are projected to the rigid-body and elastic eigenmodes by multiplication with the transposed modal matrix $\boldsymbol{\Phi}$ yielding the generalized aerodynamic forces (GAF). The modal matrix $\boldsymbol{\Phi}$ contains the eigenmodes mapped to the aerodynamic surface. Equation (7) can be solved numerically in the time domain by applying the Newmark method in combination with a staggered co-simulation coupling scheme [15]. Hence, at each time step, the modal displacements lead to grid deformations which result in updated aerodynamic forces.

For the linear analysis, equation (7) is transformed into the frequency domain assuming harmonic motion of the modal displacements $\boldsymbol{q} = \hat{\boldsymbol{q}} e^{i\omega t}$:

$$(8)\quad -\omega^2\boldsymbol{M}\hat{\boldsymbol{q}} + \boldsymbol{K}\hat{\boldsymbol{q}} = \boldsymbol{\Phi}^{\mathrm{T}}\hat{\boldsymbol{f}}_a$$

The complex-valued aerodynamic forces $\hat{\boldsymbol{f}}_a$ result from the integrated pressure distribution of the LFD solution which is obtained for the harmonic modal motion with the frequency ω.

2. NUMERICAL RESULTS

2.1. Numerical Setup

The XRF1 research model [16] is the investigated transport aircraft configuration. The cruise Mach number is 0.83 at an altitude of 10.6 km. The aerodynamic flight shape is vertically trimmed at an angle of attack of 2.0165 degree resulting in a unit vertical load factor based on the total structural mass of 198450 kg. However, the additional deformations resulting from the trimmed state are not considered in the following aerodynamic and aeroelastic simulations. Instead, the dynamic displacement $\boldsymbol{q}$ from the trimmed state is computed by artificially forcing equation (7) and (8) to be fulfilled if $\boldsymbol{q} = \boldsymbol{0}$. Nevertheless, the remaining steady aerodynamic moments around the center of gravity are very small. The steady state is summarized in TAB 1.

TAB 1. Steady flow state parameters

Parameter	*Value*
Mach number	0.83
Velocity	246.124 m/s
Angle of attack	2.0165 deg
Density	0.3796 kg/m^3
Vertical load factor	~1.0
Maximum y+	3.1

The aerodynamic model is a hybrid unstructured-structured volume mesh consisting of around 7.78 ·10^6 grid nodes with 192559 surface nodes, see FIG 1. The far-field boundary is spherical with a radius of 1000 m. The vicinity of the surface possesses a fine, structured mesh for the boundary layer, cf. FIG 2, yielding a maximum non-dimensional height of the first boundary layer cell y+ of 3.1 at the steady state condition. The engines are modelled as flow-through nacelles without thrust. FIG 3 shows the surface pressure distribution of the transonic steady state.

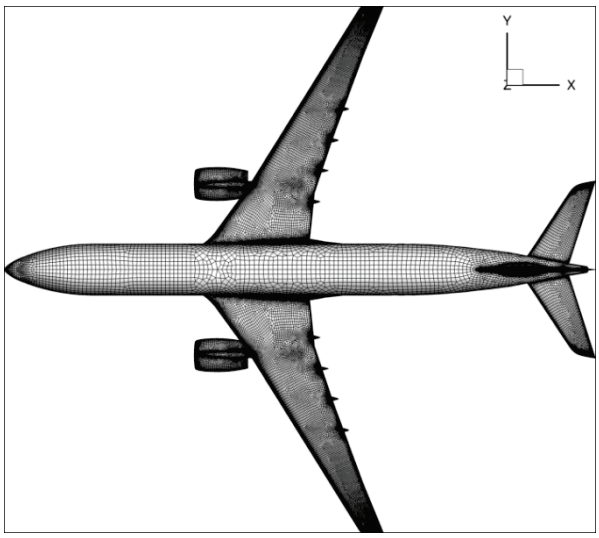

FIG 1. Surface grid of the XRF1 transport aircraft configuration.

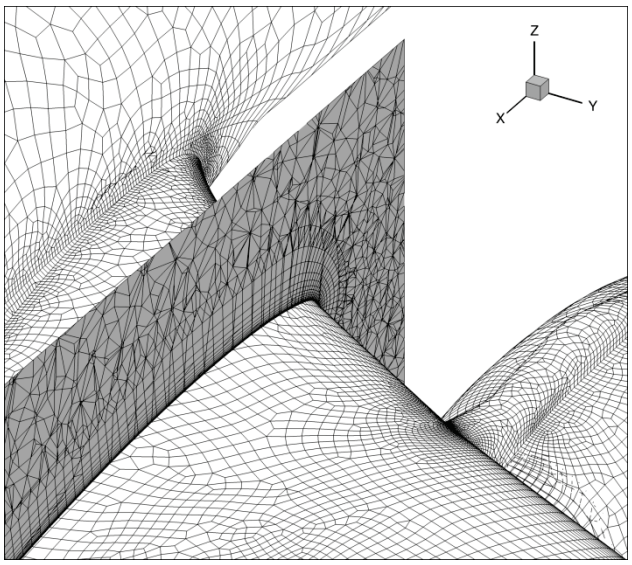

FIG 2. Surface grid at the wing root of the transport aircraft configuration and volume mesh cut displaying the structured mesh near the vicinity of the surface.

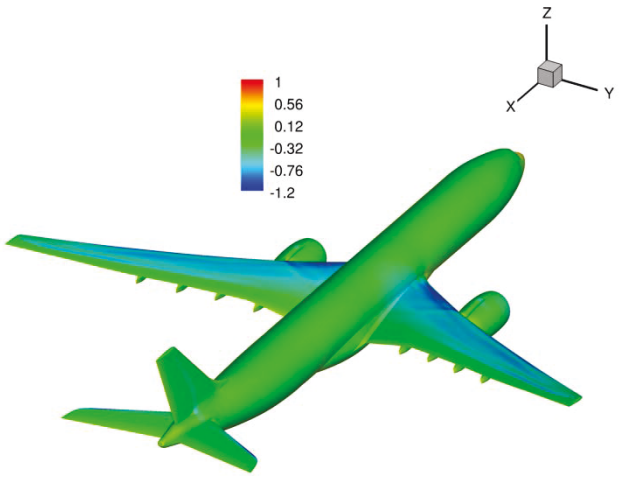

FIG 3. Distribution of the pressure coefficient on the surface of the transport aircraft configuration at the steady flow state.

The structural model of the XRF1 research model for the considered mass case is developed in [17] by means of an automated aeroelastic design process. It is a condensed finite-element model using beam elements in combination with a lumped mass model for describing of the structural dynamic behavior. A modal analysis yields the elastic eigenmodes together with the corresponding eigenfrequencies. From the set of elastic eigenmodes only the first elastic eigenmode, cf. FIG 4, with the lowest frequency is selected for the considered set of structural modes. This elastic mode is normalized to modal mass one. Additionally, two rigid-body modes, the heave and the pitch motion around the center of gravity, are included. The heave mode is scaled to an amplitude of 1 m and the pitch mode to 1 rad. These three modes allow describing the primary aircraft response to a vertical gust encounter in symmetric longitudinal flight which is sufficient for the demonstration of the aeroelastic coupling investigated in this paper. Hence, the modal mass and stiffness matrices on the left-hand side of equations (7) and (8) are defined by the parameters listed in TAB 2.

TAB 2. Structural model parameters

Parameter	*Value*
Mass	198450 kg
Inertia or rotation	2.01E7 kgm/s^2
1st eigenfrequency	1.003Hz

FIG 4. Visualization of the first elastic eigenmode mainly exposing a symmetric bending of the wings.

The examined small-amplitude gust encounter is a discrete vertical gust with a typical 1-cos shape. The gust parameters are listed in TAB 3 and the resulting time signal of the gust velocity at the nose of the aircraft is shown in FIG 5. The aircraft's nose is the starting point of the gust encounter and thus, it acts as the reference point of equation (6). For validating the time-linearized approach, a very small gust amplitude is chosen to ensure an effectively linear aerodynamic response of the nonlinear reference simulation. The aerodynamic reference solution is obtained by employing the nonlinear TAU solver in the time domain. Therefore, the TAU solver includes a gust extension which introduces the additional grid velocities at each time step as described in section 2.1. Moreover, the aeroelastic reference is obtained by solving the coupled aerodynamic and structural equations in combination with the gust extension, cf. section 2.3. The time-domain simulation parameters are listed in TAB 4.

TAB 3. Gust parameters of the vertical 1-cos gust encounter

Parameter	*Value*
Amplitude	0.43 m/s
Length	89.5 m
Velocity	246.124 m/s
Equivalent max. gust angle of attack	0.1 deg

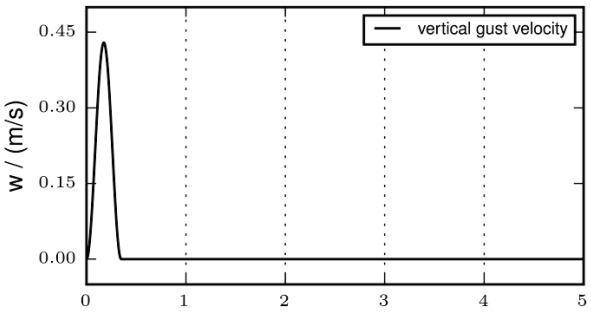

FIG 5. Time signal of the vertical gust velocity at the aircraft's nose.

TAB 4. Time-domain simulation parameters for the nonlinear reference solution

Parameter	*Value*
Time step size	0.005 s
Number of pseudo time iterations	400
CFL number (fine/coarse grid)	1.8/1.8

2.2. Generalized Aerodynamic Force Matrix

In order to compute the generalized aerodynamic forces in equation (8), harmonic moving-grid simulations of the three structural modes and harmonic gust simulations employing the LFD solver are performed. These solutions yield the force amplitudes $\hat{\boldsymbol{f}}_a$ which are further projected on the three structural modes according to the right-hand side of equation (8). The GAF matrix is assembled from four excitations which are the three modal displacements and one gust excitation. Thus, for each frequency, the FRF of the GAF matrix relates three outputs to four inputs. However, for saving computational time, the FRF is computed only for a small set of frequencies and the results for the remaining frequencies are reconstructed by interpolation using piecewise monotonic cubic polynomials In FIG 7 to FIG 10 the complex-valued FRF of the GAF matrix is displayed in terms of its four columns. The markers indicate the simulated frequencies while the lines illustrate the interpolated FRF. For the examined gust encounter a set of 20 frequencies is simulated clustering at low frequencies.

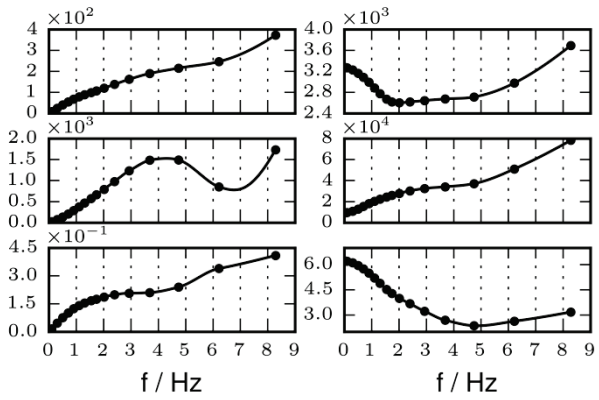

FIG 6. Absolute value of the FRF of the GAF matrix for rigid body modes heave (left) and pitch (right).

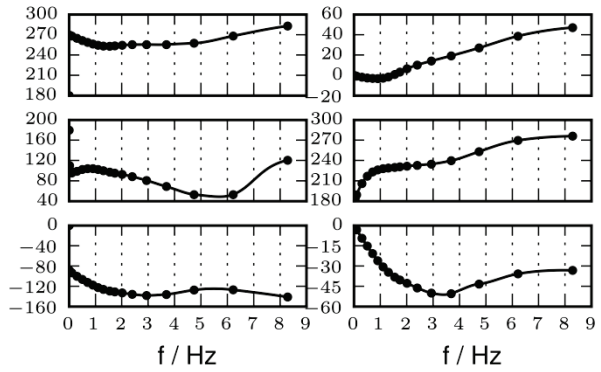

FIG 7. Phase of the FRF of the GAF matrix for the rigid body modes heave (left) and pitch (right).

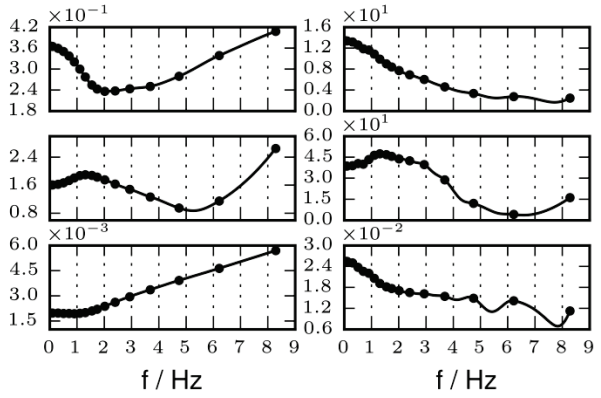

FIG 8. Absolute value of the FRF of the GAF matrix for the elastic wing bending mode (left) and the harmonic gust (right).

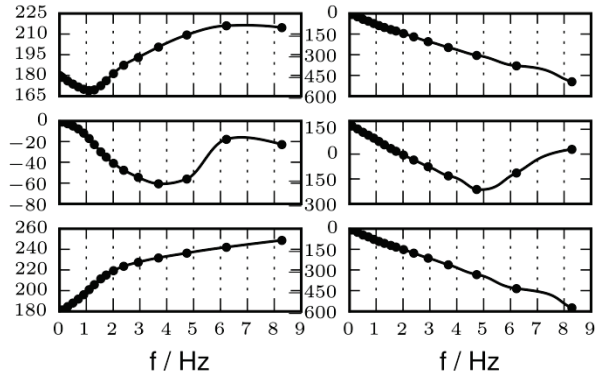

FIG 9. Phase of the FRF of the GAF matrix for the elastic wing bending mode (left) and the harmonic gust (right).

2.3. Linearized Aerodynamic Gust Response

The linearized aerodynamic response is obtained by the convolution of the gust excitation signal with the frequency response function (FRF) of the GAF matrix. The FRF is the transfer function of the aerodynamic system as illustrated in the block diagram in FIG 6. In the frequency domain, the convolution is computed by the multiplication of the transfer function with the Fourier transformed input signal:

(9) $\hat{\boldsymbol{f}}(\omega) = \boldsymbol{A}(\omega)\hat{\boldsymbol{q}}_{gust}(\omega)$

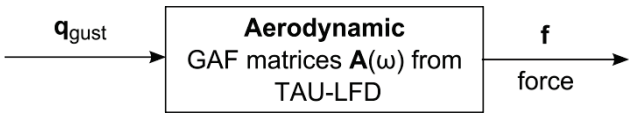

FIG 10. Aerodynamic system in the frequency domain with gust excitation.

Therefore, the linearized aerodynamic gust response results from the convolution of the GAF matrix with the discrete Fourier transformed [19] excitation signal of the gust in FIG 5. Hence, the gust input signal excites only the last column of the GAF matrix which comprises the harmonic gust solutions. Afterwards, the result is transformed into the time domain by the inverse Fourier transform yielding the time series of the linearized aerodynamic response. The time signals of the three GAFs are displayed in FIG 11 together with the nonlinear reference solution. The signals show good agreement except for very small differences in the maximum amplitude peak and in the region of attenuation. The differences may result from both the approximation of the FRFs using interpolated values and from the differences between the linear and nonlinear approaches for the chosen gust amplitude. The aerodynamic results in FIG 11 are the forces resulting for an artificially fixed aircraft without rigid-body and elastic response. However, for visualization, the forces are projected onto the structural modes yielding the GAFs.

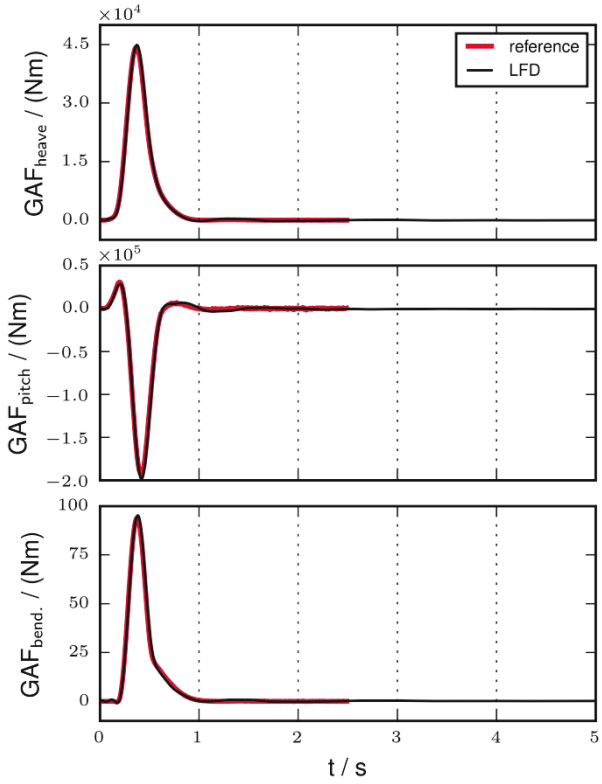

FIG 11. Time signals of the GAFs due to a small-amplitude 1-cos gust encounter for a fixed aircraft comparing the time-linearized response to the nonlinear reference solution.

2.4. Linearized Aeroelastic Gust Response

The linear aeroelastic system is constructed by extending the aerodynamic system of FIG 6 with a feedback loop involving the structural model of equation (8). The aerodynamic forces are fed back into the structural system which in turn yields modal displacements that induce additional airloads. This feedback loop as displayed in FIG 12 can be solved directly in the frequency domain yielding the coupled transfer function between the excitation amplitude $\hat{\boldsymbol{q}}_{gust}$ and the generalized force amplitude $\hat{\boldsymbol{f}}$:

$$(10)\ \hat{\boldsymbol{f}}(\omega) = \left(\boldsymbol{I} - \boldsymbol{A}(\omega)\boldsymbol{S}(\omega)\right)^{-1}\boldsymbol{A}(\omega)\hat{\boldsymbol{q}}_{gust}(\omega)$$

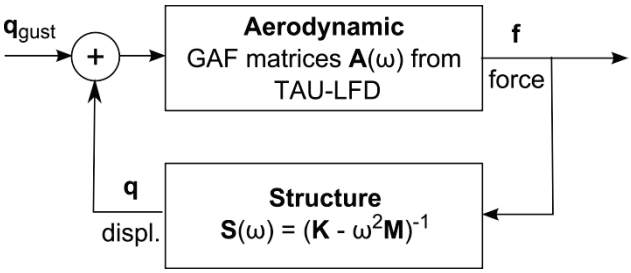

FIG 12. Aeroelastic feedback loop in the frequency domain with gust excitation.

Therefore, the aeroelastic ROM couples the structural system described by the modal mass and stiffness matrices of section 3.1 and the aerodynamic system which is identical to the sampled aerodynamic transfer functions from section 3.2. In contrast to the previous section, due to the aeroelastic coupling, the aircraft's response is not zero anymore but includes the rigid-body and elastic degrees of freedom.

FIG 13 and FIG 14 show the aeroelastic time domain response which is obtained by applying once more the inverse Fourier transform to the convolution of the gust input signal with the transfer function of the coupled aeroelastic system. The nonlinearly obtained time domain solution is displayed for comparison. It is worthwhile noting, that the heave degree of freedom correctly experiences a permanent offset after the gust encounter, while the other modal displacements return to zero. Overall, the time signals of the time-linearized aeroelastic coupling agree well with the reference solution. In FIG 13 only small differences in the maximum amplitude peak can be noticed. In FIG 14 the time series of the modal displacements are shown with good agreement to the nonlinear reference signals. However, the second modal coordinate, the pitch angle, slowly diverges from the reference after some time, a fact which is not reflected in the pitch moment signal in FIG 13. Nevertheless, the diverged curves feature the same characteristics. Thus, this drift is most likely due to an inaccuracy in the numerical schemes of either the linearized or the nonlinear reference solution and needs further investigation.

Note that the aeroelastic reduced-order model once set up can be utilized to handle further arbitrary input signals at no extra cost. This is demonstrated for the variation of the gust wave length, see FIG 15. FIG 16 and FIG 17 show the time signals of the GAFs and modal displacements for the variation. The results are obtained by employing the identical aeroelastic ROM but varying the input signal.

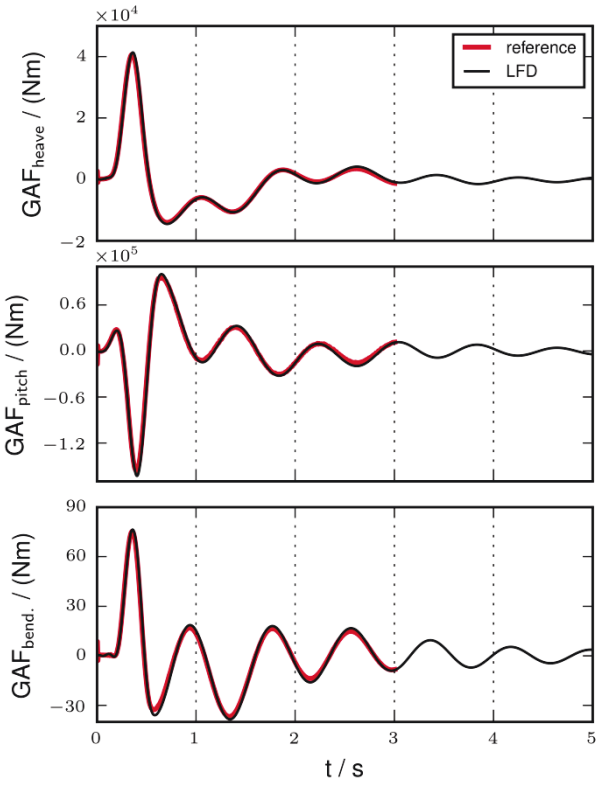

FIG 13. Time signals of the GAFs for the heave, pitch and elastic modes.

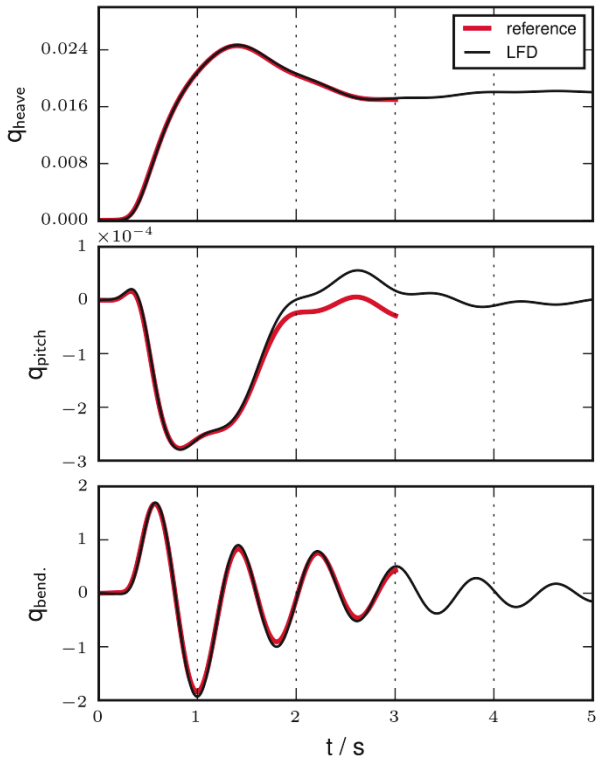

FIG 14. Time signal of the modal displacements for the heave, pitch and the elastic mode.

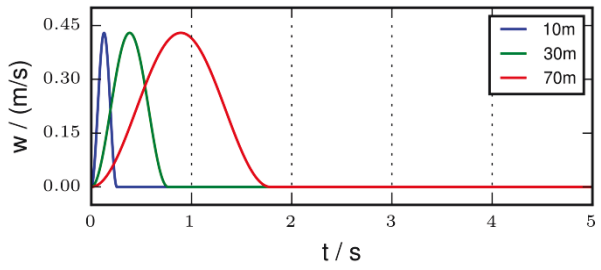

FIG 15. Time signal of the vertical gust velocity for different gust wave lengths at the aircraft's nose.

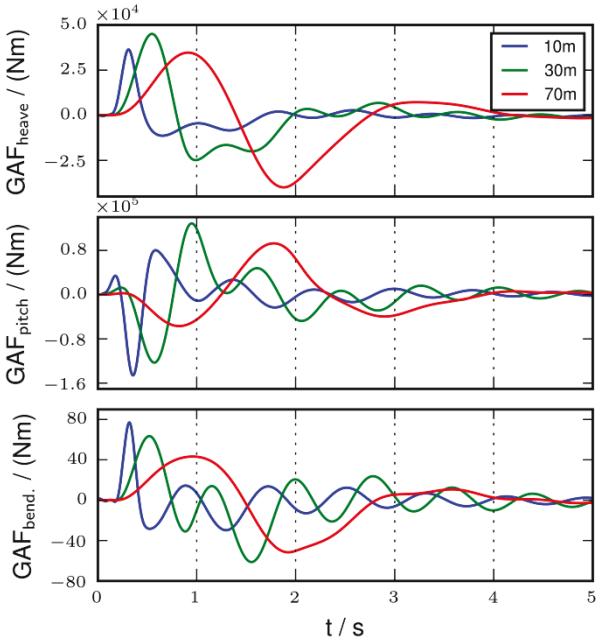

FIG 16. Time signals of the GAFs for the heave, pitch and elastic modes.

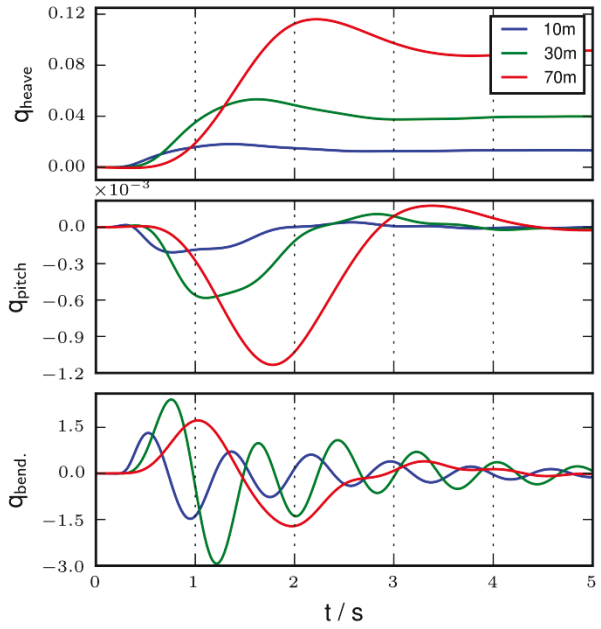

FIG 17. Time signal of the modal displacements for the heave, pitch and the elastic mode.

3. CONCLUSION

The aerodynamic and aeroelastic response due to a 1-cos gust encounter of the XRF1 transport aircraft is investigated using time-linearized aerodynamic and aeroelastic reduced-order models. The aeroelastic response comprises both rigid-body motion and elastic deformation of the aircraft. The validation is performed by comparison of the linear and the nonlinear time-domain results. Very good agreement is achieved. The aerodynamic and aeroelastic analysis shows the fidelity of the time-linearized approach.

For computing the aerodynamic FRFs a set of 20 frequencies is used. The computational time for this set exceeds the time of one single time-domain simulation by a factor of 6, but the linearly obtained time signal can be computed for much longer periods and more importantly, the computed FRF can be used for encounters of arbitrary gust shapes and further linear aeroelastic analysis.

The results presented in this paper are part of the DLR internal project Digital-X [16].

REFERENCES

[1] Albano, E., Rodden, W.P.: A Doublet-Lattice Method for Calculating Lift Distributions on Oscillating Surfaces in Subsonic Flows. AIAA Journal, Vol. 7, No. 2, 1969, pp. 279–285

[2] Thormann R., Widhalm M.: Linear-Frequency-Domain Predictions of Dynamic-Response Data for Viscous Transonic Flows, AIAA Journal Vol. 51, No. 11, 2013

[3] Chassaing, J.C., Gerolymos, G.A.: Time-Linearized Time-Harmonic 3-D Navier–Stokes Shock-Capturing Schemes. International Journal for Numerical Methods in Fluids, Vol. 56, No. 3, 2008, pp. 279–303

[4] Schwamborn, D., Gerhold, T., Heinrich, R.: The DLR TAU-Code: Recent Applications in Research and Industry. In proceedings of European Conference on Computational Fluid Dynamics, ECCOMAS CDF, Delft, The Netherland, 2006

[5] Spalart P.R., Allmaras S.R.: A One-Equation Turbulence Model for Aerodynamic Flows. In 30th Aerospace Sciences Meeting and Exhibit, January 1992

[6] Jameson A: Time Dependent Calculations Using Multigrid, with Applications to Unsteady Flows Past Airfoils and Wings. In 10th Computational Fluid Dynamics Conference, Honululu, 24–26 June, 1991

[7] Hirt, C. W., Amsden A. A., Cook, J. L.: An Arbitrary Lagrangian-Eulerian Computing Method for All Flow Speeds. Journal of Computational Physics 14, 1974, pp. 227-53

[8] de Boer, A., van der Schoot, M.S., Bijl, H.: Mesh Deformation Based on Radial Basis Function Interpolation. Computers & Structures, Vol. 85, No. 2, 2007, pp. 784–795

[9] Singh, R., Baeder, J.D.: The Direct Calculation of Indicial Lift Response of a Wing Using Computational Fluid Dynamics. Journal of Aircraft, Vol. 35, No. 4, 1997, pp. 465–471

[10] Heinrich R., Michler A.: Unsteady Simulation of the Encounter of a Transport Aircraft with a Generic Gust by CFD Flight Mechanics Coupling. CEAS Conference, Menchester UK, 2009

[11] Dwight, R., Brezillon, J., Vollmer, D.B.: Efficient Algorithms for Solution of the Adjoint Compressible Navier–Stokes Equations with Applications. In Proceedings of the 7th ONERA-DLR Aerospace Symposium, edited by ODAS, Toulouse, France, 2006, pp. 1–11

[12] Kaiser, C., Thormann, R., Dimitrov, D., Nitzsche, J.: Time-Linearized Analysis of Motion-Induced and Gust-Induced Airloads with the DLR TAU Code. In: Deutscher Luft- und Raumfahrtkongress, 2015, Rostock, Germany.

[13] Saad, Y., Schultz, M.H.: GMRES: A Generalized Minimum Residual Algorithm for Solving Nonsymmetric Linear Systems. SIAM Journal on Scientific and Statistical Computing, Vol. 7, No. 3, 1986, pp. 856–859.

[14] McCracken, A.J., Timme, S., Badcock, K.J.: Accelerating Convergence of the CFD Linear Frequency Domain Method by a Preconditioned Linear Solver. In Proceedings of 6th European Congress on Computational Methods in Applied Sciences and Engineering, edited by Eberthardsteiner et. al., ECCOMAS 2012, Vienna, Austria, Sept. 2012

[15] Neumann, J., Nitzsche, J., Voß, R.: Aeroelastic Analysis by Coupled Non-Linear Time Domain Simulation. In: Proceedings - AVT-154 Specialists Meeting on Advanced Methods in Aeroelasticity. AVT-154 Specialists Meeting on Advanced Methods in Aeroelasticity, 2008, Loen, Norway.

[16] Kroll, N., et al.: DLR project Digital-X: towards virtual aircraft design and flight testing based on high-fidelity methods. CEAS Aeronaut Journal, Vol. 7, 2016, pp. 3–27

[17] Liepelt, R., Handojo, V., Klimmek, T.: Aeroelastic Analysis Modelling Process To Predict The Critical Loads In An MDO Environment. International Forum on Aeroelasticity and Structural Dynamics (IFASD), 2015, Saint Petersburg, Russia.

[18] Cooley, J.W., Tukey, J.W.: An algorithm for the machine calculation of complex Fourier series. Math. Comput. 19: 297-301, 1965